All Sciences Proceedings

5th International Conference on Applied Engineering and Natural Sciences

July 10-12, 2023 : Konya, Turkey

All Sciences Proceedings
http://as-proceeding.com/

https://www.icaens.com/

Numerical Comparison of Active Shielding Techniques for Magnetic Fluid Hyperthermia Application

Serhat Küçükdermenci [*,1]

[1]Department of Electrical and Electronics Engineering, Faculty of Engineering, Balıkesir University, 10463, Balikesir, Turkey.

[*](kucukdermenci@balikesir.edu.tr) Email of the corresponding author

Abstract –This study aims to eliminate magnetic field leakage at 100 kHz with active shielding in Magnetic Fluid Hyperthermia (MFH) system. First of all, the structural and operational features of the MFH system were analyzed. Then, the active regions of the coils were determined, graphical results were obtained and the designs were compared with each other. We first simulated the magnetic field distribution of a circular coil active shielding system by the commercial software tool COMSOL Multiphysics. Secondly, a single D-shape shielding was configured in the MFH system and the size and location of the shielding were examined. The magnetic field attenuation percentages of the methods in the x, y, z axes and the target region selected as the representative tumor region were compared. The simulation results show that the shielding ability of the double D-shape shielding type is better in the x and y axes than the other coil types (51.43% for the x-axis and 95.77% for the y-axis). The fact that the attenuation percentage of this shielding type in the target region is 0.0287% is a secondary advantage. It has been observed that the attenuation in the z-axis is higher in other shielding types, but the attenuation percentage in the target region also increases.

Keywords – Active Shielding, Magnetic Hyperthermia, High Frequency Magnetic Field, Electromagnetic Compatibility, Magnetic Area, Near Field;

I. INTRODUCTION

Magnetic fields have recently been widely used for both diagnostic and therapeutic purposes in various bioengineering and biomedical applications. In more detail, one of the most relevant advantages over existing technologies is the lower invasiveness on patients, especially with regard to non-ionizing radiations. In addition, due to the non-magnetic nature of human tissues, the tissue-air interface does not interfere with the penetrating magnetic field, unlike its electric field counterpart. Various diagnostic and treatment methodologies such as Magnetic Resonance Imaging (MRI) [1], hyperthermia and thermo-ablation with magnetic nanoparticles (also called Magnetic Fluid Hyperthermia, MFH) [2], and Transcranial Magnetic Stimulation (TMS) [3] use this physical entity. In these biomedical applications, the desired magnetic field distribution of Radio Frequency (RF) plays a relevant role to increase the effectiveness of the procedure, and its distribution is relevant to the purpose of the particular technologies.

The biology of many cancer types are significantly influenced by exposure to risk factors, making cancer the second most common cause of death in the world [4]. Chemotherapy, surgery, and radiation therapy are common treatments. However, significant side effects in healthy tissues have been observed during or after these therapies [5]. Furthermore, in some circumstances, the tumor location is inaccessible for surgery, or the tumor may not respond properly to chemo or radiation therapy. In such circumstances, an alternate technique is to use hyperthermia, which exposes the tumor to temperatures higher than normal body temperature.

Magnetic fluid hyperthermia (MFH) therapy is a type of thermotherapy that uses MNPs deposited in tumor tissues and creates a friction resulting from magnetic moment rotation (Ne´el relaxation) and nanoparticle rotation induced by alternating magnetic field (Brownian relaxation) [6] to surrounding tissues or to provide local heat to organs [7]. This heat can raise the local tissue temperature above 43˚C and cause cancer cells to undergo apoptosis or necrosis without significant damage to normal cells (see Figure 1). It has also been proven that thermal effects can prevent tumor cells from recovering from DNA damage [8]. Conversely, normal cells may remain intact during thermotherapy; side effects in hyperthermia treatments are therefore less than in chemotherapy or radiotherapy [9].

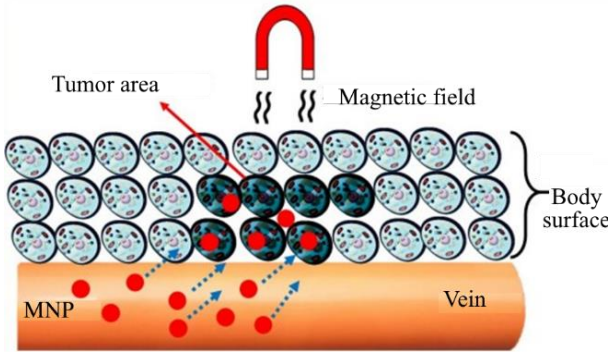

Fig. 1 Magnetic fluid hyperthermia

In the MH treatment method, cancerous cells and healthy cells are exposed to a magnetic field. The magnetic field frequency (f) and amplitude (H) to which humans are exposed is limited. This limit is as shown in the equation (1).

$$H \times f \leq 4.85 \times 10^{8} \frac{A}{ms} \tag{1}$$

This safety conditions established by the H × f product was proposed by Atkinson–Brezovich [10], as a limit for MH therapies. Defining an appropriate safety limit became critical in order to maintain patient safety while optimizing MNP heating. Various safety restrictions have been proposed over the previous few decades, however there is still debate on the subject [11].

Therefore, in the treatment of hyperthermia, it is necessary to limit or reduce the magnetic field value that people will be exposed to. A shielding system has been considered to solve this situation.

Passive shielding is the optimization of the magnetic channel by exploiting magnetic materials' magnetic conductivity or the generation of reverse MF by eddy current produced by conductive metal materials in high frequency MF to reduce MF leakage [12], [13], [14]. The Al-plate passive shielding [15], [16], [17] is extensively utilized for stationary electric vehicle (EV) wireless charging applications, regardless of whether the coil structure is a simple circular pad [18], DD pad [19], [20], DDQ pad [21], or even bipolar pad [22].

Active shielding is a relatively new concept, yet it can provide effective shielding in the WPT system. In some circumstances with a significant air gap, the horizontal leakage magnetic field cannot be ignored. To remove or lessen the leaking MF, the suppression coil with excitation source generates the offset magnetic field opposite to the original magnetic field [23], [24]. The shielding effect is visible in a dynamic wireless charging system, however this way is detrimental to the overall efficiency of the system, so a proper shielding plan must be designed [25], [26].

The aim of this study is to design shielding systems in simulation environment to reduce or limit the high frequency magnetic field values produced for MFH, which is one of the biomedical applications. The attenuation effects of the shielding designs created in the simulation environment were measured and the effects in the study area were compared.

II. Materials and Method

In this section, shielding designs for magnetic field generator are simulated using the Comsol Multiphysics 5.6 simulation software. An overview of the components in the workspace is shown in Figure 2. Tumor measurement points determined as target points are in the Z-axis and 45 mm from the source coil center.

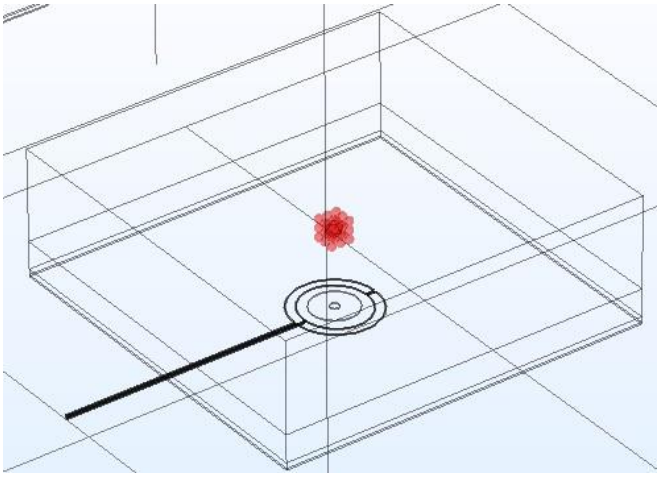

Fig. 2 An overview of the components in the workspace.

A representative living tissue consisting of epidermis, dermis, fat, healthy tissue and tumor was placed on this system. In the materials section, the coils are assigned as copper. The values in Table 1 were used for representative living tissue [27].

Table 1. Living tissue material values.

Layers	Density (kg⁄m^3)	Specific Heat (J/kg-K)	Conductivity (W/m-K)
Healthy Tissue	1000	2540	0.642
Tumor	1660	3720	0.788
Fat	2000	6500	0.69
Dermis	1200	3300	0.45
Epider mis	1200	3590	0.24

The measurement points in red color in Figure 3 are placed on the X-axis starting from the origin point up to 500 mm at 10 mm intervals. In addition, a 1D plot group measurement line has been added, extending along the x-axis from the origin to 700 mm.

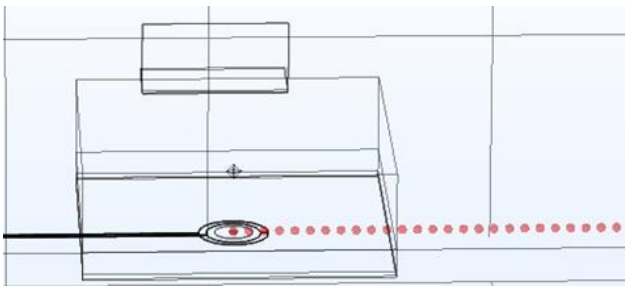

Fig. 3 Measuring points positioned on the X-axis.

Similarly, the measurement points shown in red in Figure 4 are spaced 10 mm apart on the Y axis starting from the origin point up to 500 mm. In addition, a 1D plot group measurement line has been added, extending from the origin to 1000 mm along the x-axis.

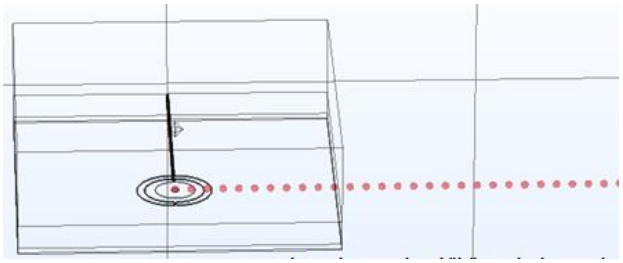

Fig. 4 Measuring points positioned on the Y-axis.

A. *Active Shielding with the Circular Coil*

In this type of shielding made by using a circular coil, pancake shaped coil winding is used as the magnetic field source. The inner radius of the coil is 10 mm, the outer radius is 50 mm, and the coil consists of 15 turns. For active shielding, a circular shaped coil consisting of 4 turns with an inner radius of 60 mm and an outer radius of 70 mm was designed as shown in Figure 5.

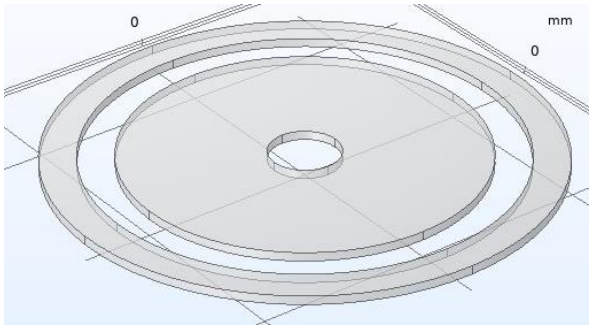

Fig. 5 Active shielding with the circular coil

The current value is 55.1 amperes (A) for the source coil producing high frequency alternating magnetic field, and 50 A is used for the shielding coil. The operating frequency of the system is 100 kHz. Measurements were taken on the X, Y, Z axis, and on the tumor, with and without shielding in the simulation.

Equation (2) and (3) were used for the measurements [28]. The shielding effect was observed and the shielding effect value (SEV) was measured in all axes.

$$B_{total} = B_{source} + B_{shield} \tag{2}$$

$$SEV = (1 - \frac{B_{total}}{B_{source}}) \times 100 \tag{3}$$

B. *Active Shielding with Single D-Shaped Coil*

A different active shielding coil design was applied for the high frequency alternating magnetic field source created earlier. The inner radius value of the coil in Figure 6 is 70 mm, and the outer radius value is 90 mm.

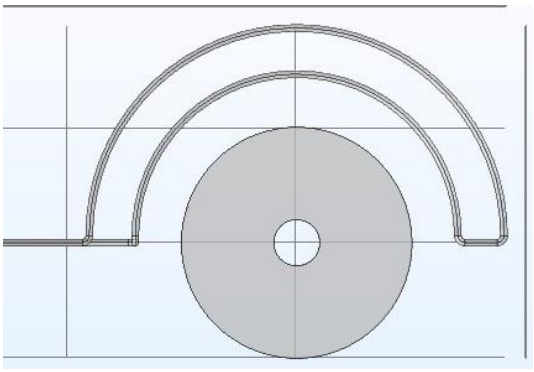

Fig. 6 Active shielding with the single D-shaped coil

A current supply of 55.1 A for the coil that is the source of the magnetic field and 50 A for the shielding coil is applied. The system created in the simulation environment was operated at 100 kHz. Measurements were taken on the system without using shielding and with using shielding.

C. *Active Shielding with Double D-Shaped Coil*

The previous shielding work was applied to the high frequency alternating magnetic field source with two coils as shown in Figure 7. The magnetic field source coil was fed with the same current values. Both shielding coils have an inner radius of 70 mm and an outer radius of 90 mm.

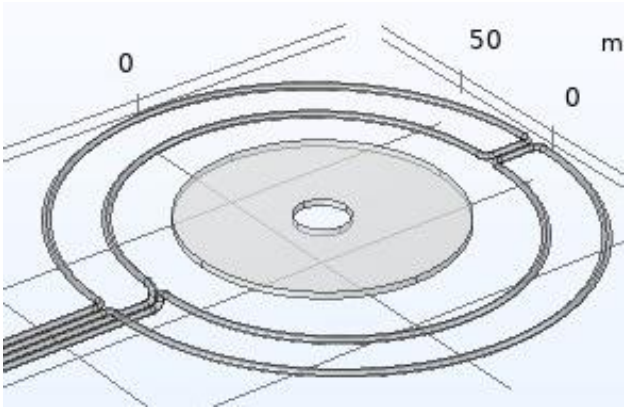

Fig. 7 Active Shielding with Double D-Shaped Coil

A current supply of 55.1 A for the coil that is the source of the magnetic field and 50 A for the shielding coil is applied. The system created in the simulation environment was operated at 100 kHz. Measurements were taken on the system without using shielding and with using shielding.

III. RESULTS

Flux density maps for active shielding for the circular coil with and without shielding effect are shown in Figure 8a-f, and 1D plot group drawings are shown in Figure 9a-f.

For the circular coil, the highest shielding effect value in the X-axis was found to be 99.0267% at a distance of 500 mm from the center. The shielding effect in the X-axis started at a distance of 20 mm from the active shielding coil. The shielding effect value at the starting point of the shielding effect was found to be 17.6641%. The highest shielding effect value in the Y axis was found to be 98.835% at a distance of 500 mm from the active shielding coil. The shielding effect started at a distance of 20 mm from the active shielding coil and the shielding effect value was found to be 14.8708%. The highest shielding effect value in the Z axis was found to be 91.4373% at a distance of 220 mm from the center of the system. The shielding effect started from the center of the system and the shielding effect value was found to be 9.6008%.

The 2D plot groups of the flux density maps for active shielding with single D-shaped coil are shown in Figure 10a-f, and 1D plot group drawings for magnetic flux density distance graphs are shown in Figure 11a-f.

For the single D-shaped coil, the magnetic field to which the target point is exposed has decreased. The highest shielding effect value in the X-axis was found to be 80.3535% at a distance of 10 mm from the active shielding coil. The shielding effect started at a distance of 90 mm from the center and the shielding effect value was found to be 22.4816%. The highest shielding effect value in the Y axis was found to be 88.114% at a distance of 20 mm from the active shielding coil. The shielding effect value in the Y-axis started at a distance of 20 mm from the active shielding coil. The shielding effect in the Z axis started at a distance of 40 mm from the center and the shielding effect value was found to be 7.2370%. The highest shielding effect value was found as 19.8581% at a distance of 240 mm from the center.

The 2D plot groups of the flux density maps for active shielding with double D-shaped coil are shown in Figure 12a-f, and 1D plot group drawings

for magnetic flux density distance graphs are shown in Figure 13a-f.

For the double D-shaped coil, the highest shielding effect value in the X axis was measured as 71.0652% at a distance of 20 mm from the active shielding coil. The shielding effect started at a distance of 10 mm from the active shielding coil and the shielding effect value was found to be 51.4277. The highest shielding effect value in the Y-axis was measured as 95.7713% at a distance of 20 mm from the active shielding coil. The shielding effect value started at a distance of 20 mm from the active shielding coil. The shielding effect in the Z axis started at a distance of 40 mm from the center of the system. The highest shielding effect value in the Z axis was measured as 4.6072% at 110 mm distance from the center of the system. The shielding effect in the Z axis started at a distance of 40 mm from the center of the system and the shielding effect value was found to be 0.9746%.

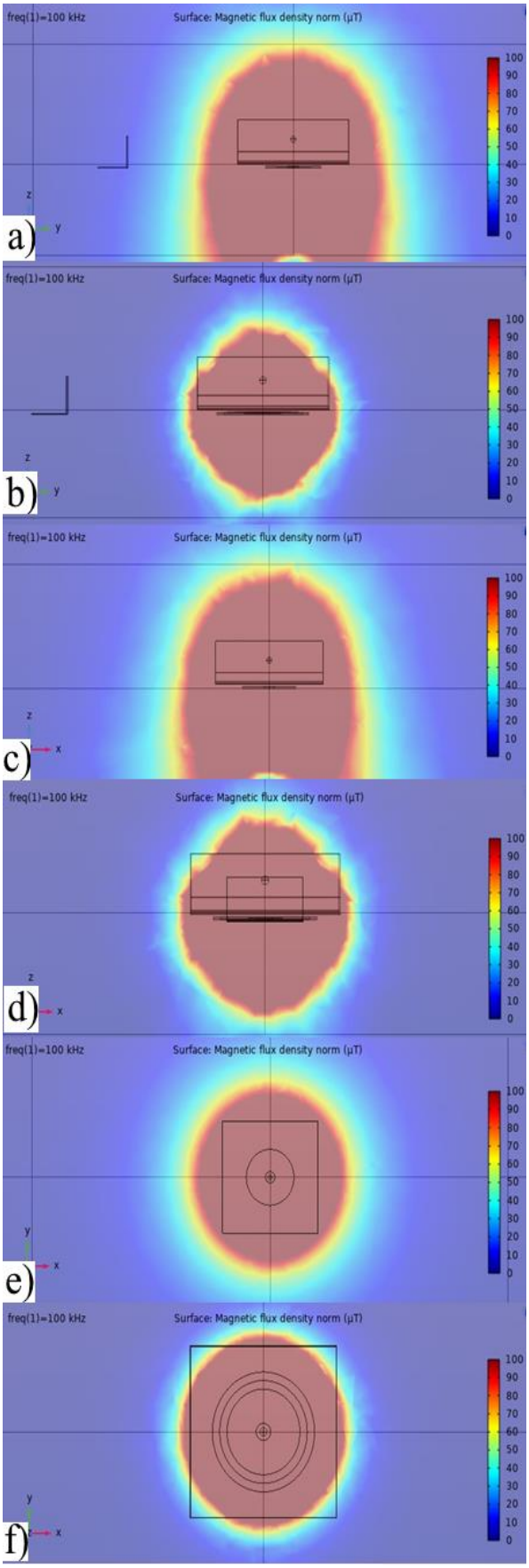

Fig. 8 Flux density maps for active shielding with the circular coil a) without shielding b) with shielding on the X-axis, c) without shielding d) with shielding on the Y-axis, e) without shielding f) with shielding on the Z-axis.

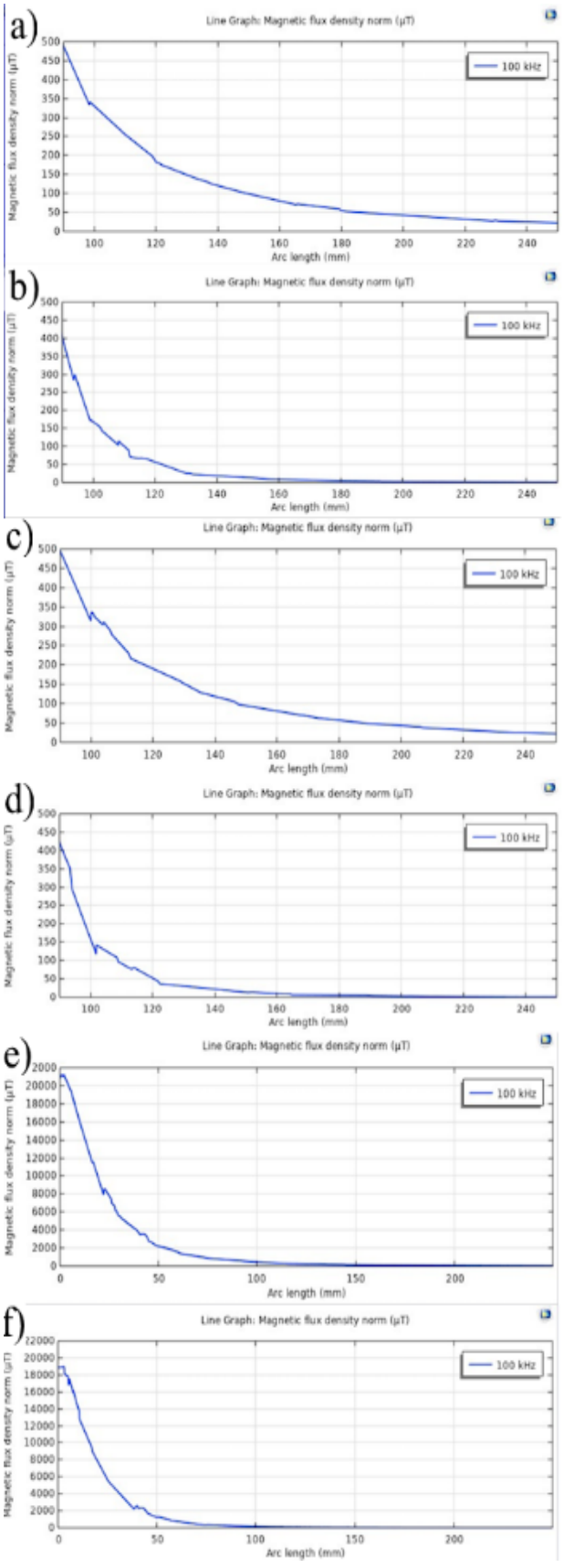

Fig. 9 Magnetic flux density distance graphs for active shielding with the circular coil a) without shielding b) with shielding on the X-axis, c) without shielding d) with shielding on the Y-axis, e) without shielding f) with shielding on the Z-axis.

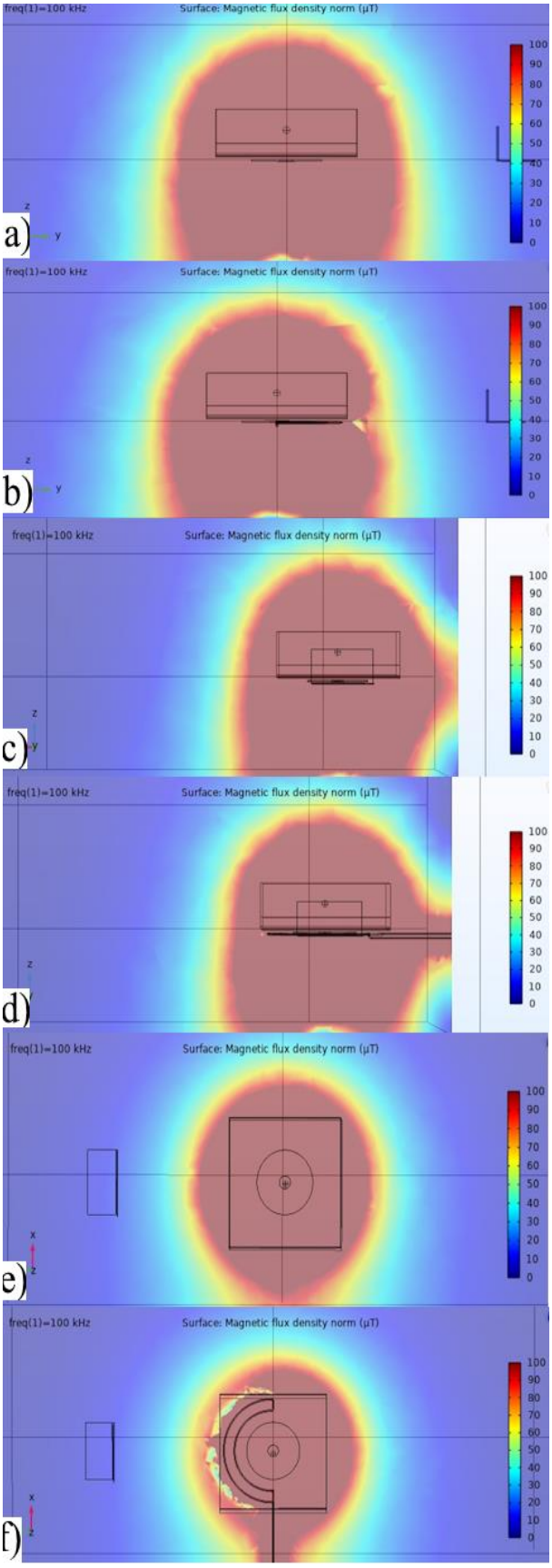

Fig. 10 Flux density map for active shielding with a single D-shaped coil a) without shielding b) with shielding on the X-axis, c) without shielding d) with shielding on the Y-axis, e) without shielding f) with shielding on the Z-axis.

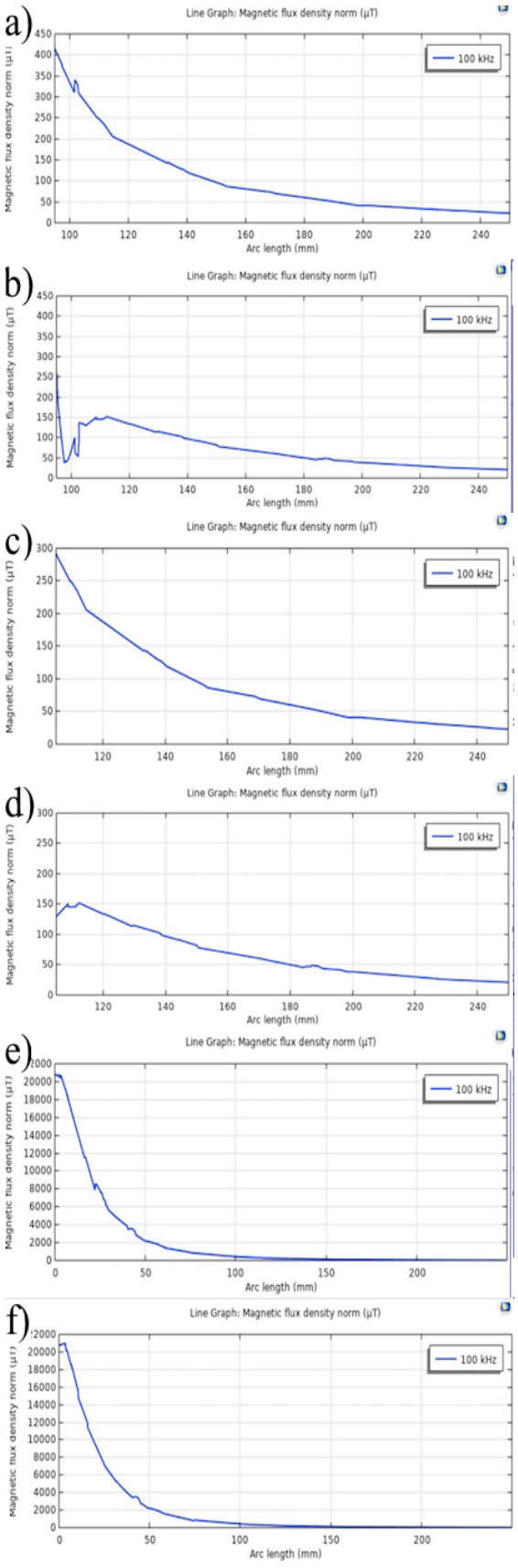

Fig. 11 Magnetic flux density distance graphs for active shielding with a single D-shaped coil a) without shielding b) with shielding on the X-axis, c) without shielding d) with shielding on the Y-axis, e) without shielding f) with shielding on the Z-axis.

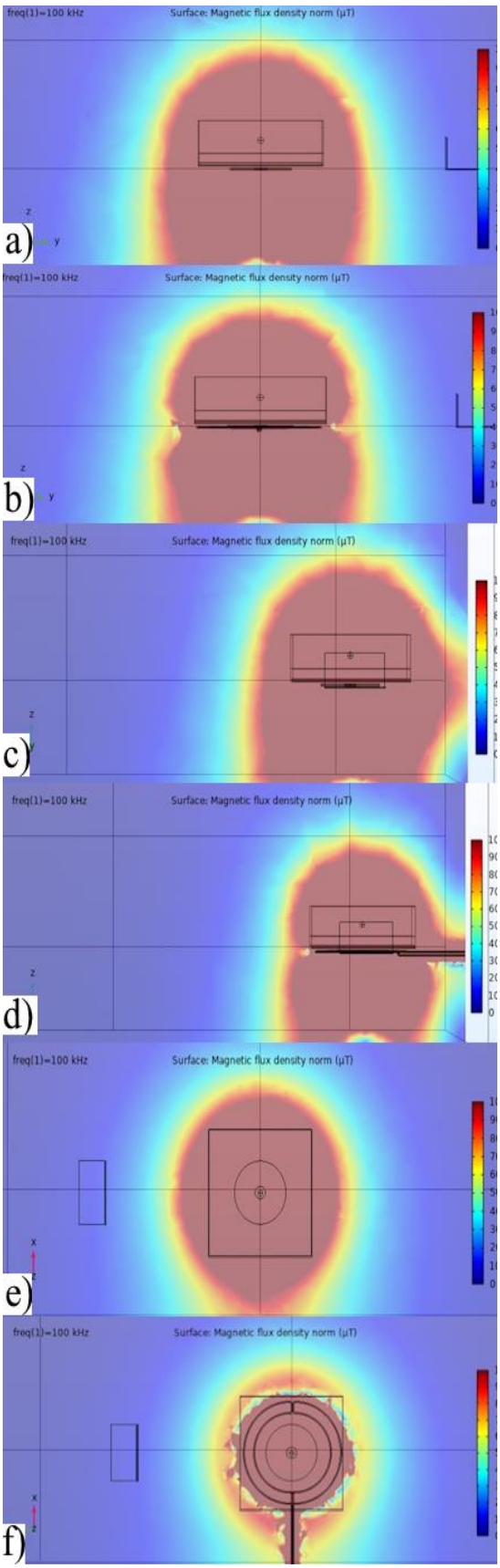

Fig. 12 Flux density map for active shielding with double D-shaped coil a) without shielding b) with shielding on the X-axis, c) without shielding d) with shielding on the Y-axis, e) without shielding f) with shielding on the Z-axis.

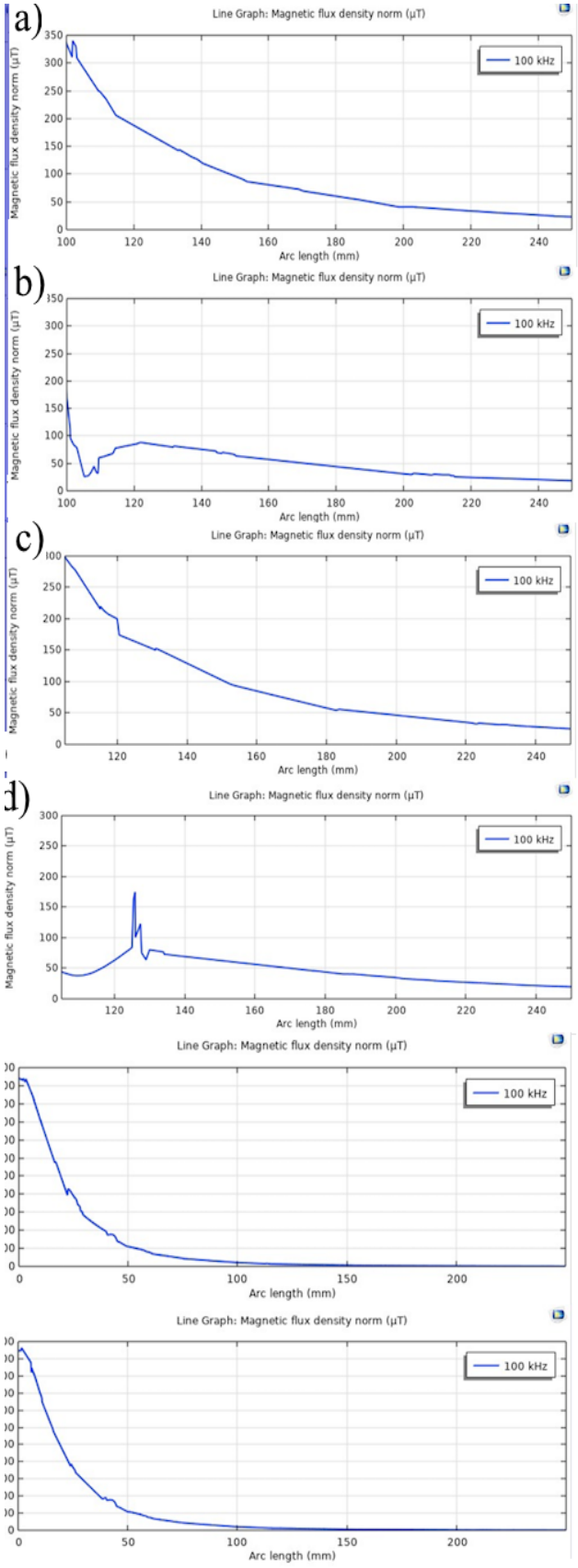

Fig. 13 Magnetic flux density distance graphs for active shielding with a single D-shaped coil a) without shielding b) with shielding on the X-axis, c) without shielding d) with shielding on the Y-axis, e) without shielding f) with shielding on the Z-axis.

IV. DISCUSSION

For active shielding with the circular coil, the magnetic field performance of the source coil in the target region has decreased due to the opposite magnetic field produced by the active shielding coil. The effective shielding value in the tumor region, which is 45 mm from the center of the system, was calculated as 37.3157%. This difference can be considered as a disadvantage of the circular coil shielding method.

When active shielding with a single D-shaped coil is used, it is seen that the performance loss at the target point is reduced compared to active shielding with circular coils. The target point, the tumor, is located on the Z-axis at a distance of 45 mm from the center and the shielding effect value was found as 1.3051%.

For the double D-shaped coil, the shielding effect value measured on the tumor, which is 45 mm from the center of the system, was calculated as 0.9746%.

V. CONCLUSION

As seen in Table 2, circular coil reduces the performance of high frequency alternating magnetic field source by applying an attenuation of 37.3157% in the tumor region with the circular active shielding coil. It attenuates the magnetic field by 17.6641% in the X-axis. This ratio was calculated as 14.8708% in the Y-axis and 9.6008% in the Z-axis.

Table 2. Comparison of shielding effect according to coil types.

Active shielding coil type	**X-axis**	**Y-axis**	**Z-axis**	**Tumor area**
Circular coil	17.6641%	14.8708%	9.6008%	37.3157%
Single D shaped coil	22.4816%	88.1104%	7.2370%	1.3051%
Double D shaped coil	51.4277%	95.7713%	0.9746%	0.0287%

The single D-shaped active shielding coil applied a shielding of 1.3051% at the tumor site, resulting in a lower impact on the performance of the system compared to the circular coil. While the magnetic field began to attenuate by 22.4816% in the X-axis,

this rate was calculated as 88.114% in the Y-axis and 7.2370% in the Z-axis. This proves that the s ingle D-shaped active shielding coil will provide protection in areas that are 20 mm away from the active shielding coil in the X axis and 20 mm from the active shielding coil in the Y axis.

The double D-shaped active shielding coil affected the high frequency alternating magnetic performance at the tumor site by 0.0287%. Among these designs, the double D-shaped active shielding coil has the least effect on the high frequency alternating magnetic field performance. This shielding tack has proven to provide protection in areas 10 mm away from the active shielding coil in the X axis by attenuating 51.4277 percent of the magnetic field. It has proven that it will provide protection at a distance of 20 mm from the active shielding coil by performing an attenuation of 95.7713% in the Y axis.

As a result, considering the high frequency alternating magnetic field performance and shielding, it is seen that the double D-shaped active shielding design is the most suitable design for shielding magnetic field generators among shielding designs.

Magnetic hyperthermia experimental designs may differ according to the intended use. For test tubes, guinea pigs and humans, the shielding types set forth in this study can be preferred according to the intended use. These designs created in the simulation environment can be produced in the physical environment.

ACKNOWLEDGMENT

We would like to thank Necdet Özkan for the helpful discussions.

REFERENCES

[1] Y. Lu *et al.*, "Combining magnetic particle imaging and magnetic fluid hyperthermia for localized and image-guided treatment," *Int. J. Hyperth.*, vol. 37, no. 3, pp. 141–154, Dec. 2020, doi: 10.1080/02656736.2020.1853252.

[2] P. Chandrasekharan *et al.*, "Using magnetic particle imaging systems to localize and guide magnetic hyperthermia treatment: tracers, hardware, and future medical applications," *Theranostics*, vol. 10, no. 7, pp. 2965–2981, 2020, doi: 10.7150/thno.40858.

[3] L. I. Navarro de Lara *et al.*, "A novel coil array for combined TMS/fMRI experiments at 3 T," *Magn. Reson. Med.*, vol. 74, no. 5, pp. 1492–1501, Nov. 2015, doi: 10.1002/mrm.25535.

[4] J. M. Kocarnik *et al.*, "Cancer Incidence, Mortality, Years of Life Lost, Years Lived With Disability, and Disability-Adjusted Life Years for 29 Cancer Groups From 2010 to 2019," *JAMA Oncol.*, vol. 8, no. 3, p. 420, Mar. 2022, doi: 10.1001/jamaoncol.2021.6987.

[5] R. Baskar, K. A. Lee, R. Yeo, and K.-W. Yeoh, "Cancer and Radiation Therapy: Current Advances and Future Directions," *Int. J. Med. Sci.*, vol. 9, no. 3, pp. 193–199, 2012, doi: 10.7150/ijms.3635.

[6] M. Osaci and M. Cacciola, "A study of Brownian relaxation time in magnetic nanofluids: a semi-analytical model," *Multiscale Multidiscip. Model. Exp. Des.*, Jun. 2023, doi: 10.1007/s41939-023-00174-9.

[7] S. Laurent, S. Dutz, U. O. Häfeli, and M. Mahmoudi, "Magnetic fluid hyperthermia: Focus on superparamagnetic iron oxide nanoparticles," *Adv. Colloid Interface Sci.*, vol. 166, no. 1–2, pp. 8–23, Aug. 2011, doi: 10.1016/j.cis.2011.04.003.

[8] Y. Yagawa, K. Tanigawa, Y. Kobayashi, and M. Yamamoto, "Cancer immunity and therapy using hyperthermia with immunotherapy, radiotherapy, chemotherapy, and surgery," *J. Cancer Metastasis Treat.*, vol. 3, no. 10, p. 218, Oct. 2017, doi: 10.20517/2394-4722.2017.35.

[9] T. Kobayashi, "Cancer hyperthermia using magnetic nanoparticles," *Biotechnol. J.*, vol. 6, no. 11, pp. 1342–1347, Nov. 2011, doi: 10.1002/biot.201100045.

[10] W. J. Atkinson, I. A. Brezovich, and D. P. Chakraborty, "Usable Frequencies in Hyperthermia with Thermal Seeds," *IEEE Trans. Biomed. Eng.*, vol. BME-31, no. 1, pp. 70–75, Jan. 1984, doi: 10.1109/TBME.1984.325372.

[11] B. Herrero de la Parte *et al.*, "Proposal of New Safety Limits for In Vivo Experiments of Magnetic Hyperthermia Antitumor Therapy," *Cancers (Basel).*, vol. 14, no. 13, p. 3084, Jun. 2022, doi: 10.3390/cancers14133084.

[12] L. Zhai, G. Zhong, Y. Cao, G. Hu, and X. Li, "Research on Magnetic Field Distribution and Characteristics of a 3.7 kW Wireless Charging System for Electric Vehicles under Offset," *Energies*, vol. 12, no. 3, p. 392, Jan. 2019, doi: 10.3390/en12030392.

[13] M. Mohammad, E. T. Wodajo, S. Choi, and M. E. Elbuluk, "Modeling and Design of Passive Shield to Limit EMF Emission and to Minimize Shield Loss in Unipolar Wireless Charging System for EV," *IEEE Trans. Power Electron.*, vol. 34, no. 12, pp. 12235–12245, Dec. 2019, doi: 10.1109/TPEL.2019.2903788.

[14] H. Kim *et al.*, "Coil Design and Measurements of Automotive Magnetic Resonant Wireless Charging System for High-Efficiency and Low Magnetic Field Leakage," *IEEE Trans. Microw. Theory Tech.*, pp. 1–18, 2016, doi: 10.1109/TMTT.2015.2513394.

[15] J. Kim *et al.*, "Coil Design and Shielding Methods for a Magnetic Resonant Wireless Power Transfer System," *Proc. IEEE*, vol. 101, no. 6, pp. 1332–1342, Jun. 2013, doi: 10.1109/JPROC.2013.2247551.

[16] Hwansoo Moon, Sungkyu Kim, Hyun Ho Park, and Seungyoung Ahn, "Design of a Resonant Reactive Shield With Double Coils and a Phase Shifter for

Wireless Charging of Electric Vehicles," *IEEE Trans. Magn.*, vol. 51, no. 3, pp. 1–4, Mar. 2015, doi: 10.1109/TMAG.2014.2360701.

[17] Y. Jing, S. Beiyun, Z. Zhizhen, and S. Yuewu, "Shielding effectiveness of infinite metal plate with finite thickness at oblique incident and arbitrary polarizations," in *2015 7th Asia-Pacific Conference on Environmental Electromagnetics (CEEM)*, Nov. 2015, pp. 241–245, doi: 10.1109/CEEM.2015.7368675.

[18] Q. Zhu, Y. Guo, L. Wang, C. Liao, and F. Li, "Improving the Misalignment Tolerance of Wireless Charging System by Optimizing the Compensate Capacitor," *IEEE Trans. Ind. Electron.*, vol. 62, no. 8, pp. 4832–4836, Aug. 2015, doi: 10.1109/TIE.2015.2397882.

[19] M. Budhia, J. T. Boys, G. A. Covic, and C.-Y. Huang, "Development of a Single-Sided Flux Magnetic Coupler for Electric Vehicle IPT Charging Systems," *IEEE Trans. Ind. Electron.*, vol. 60, no. 1, pp. 318–328, Jan. 2013, doi: 10.1109/TIE.2011.2179274.

[20] A. Zaheer, H. Hao, G. A. Covic, and D. Kacprzak, "Investigation of Multiple Decoupled Coil Primary Pad Topologies in Lumped IPT Systems for Interoperable Electric Vehicle Charging," *IEEE Trans. Power Electron.*, vol. 30, no. 4, pp. 1937–1955, Apr. 2015, doi: 10.1109/TPEL.2014.2329693.

[21] V. De Santis, T. Campi, S. Cruciani, I. Laakso, and M. Feliziani, "Assessment of the Induced Electric Fields in a Carbon-Fiber Electrical Vehicle Equipped with a Wireless Power Transfer System," *Energies*, vol. 11, no. 3, p. 684, Mar. 2018, doi: 10.3390/en11030684.

[22] A. Zaheer, D. Kacprzak, and G. A. Covic, "A bipolar receiver pad in a lumped IPT system for electric vehicle charging applications," in *2012 IEEE Energy Conversion Congress and Exposition (ECCE)*, Sep. 2012, pp. 283–290, doi: 10.1109/ECCE.2012.6342811.

[23] S. Cruciani, T. Campi, F. Maradei, and M. Feliziani, "Active Shielding Design for Wireless Power Transfer Systems," *IEEE Trans. Electromagn. Compat.*, vol. 61, no. 6, pp. 1953–1960, Dec. 2019, doi: 10.1109/TEMC.2019.2942264.

[24] S. Cruciani, T. Campi, F. Maradei, and M. Feliziani, "Active Shielding Applied to an Electrified Road in a Dynamic Wireless Power Transfer (WPT) System," *Energies*, vol. 13, no. 10, p. 2522, May 2020, doi: 10.3390/en13102522.

[25] T. Campi, S. Cruciani, V. De Santis, F. Maradei, and M. Feliziani, "Wireless power transfer (WPT) system for an electric vehicle (EV): how to shield the car from the magnetic field generated by two planar coils," *Wirel. Power Transf.*, vol. 5, no. 1, pp. 1–8, Mar. 2018, doi: 10.1017/wpt.2017.17.

[26] Q. Li, S. Chen, W. Wang, H. Hao, and L. Li, "Improving the efficiency of magnetic coupling energy transfer by etching fractal patterns in the shielding metals," *Front. Inf. Technol. Electron. Eng.*, vol. 17, no. 1, pp. 74–82, Jan. 2016, doi: 10.1631/FITEE.1500114.

[27] K. Chauhan, S. Tiari, and M. Mahdavi, "Numerıcal Study Of Heat Transfer In Living Tissues During Hyperthermıa Treatment Of Cancer," in *Proceeding of 3rd Thermal and Fluids Engineering Conference (TFEC)*, 2018, pp. 1127–1130, doi: 10.1615/TFEC2018.bio.022013.

[28] J. Kim, J. Ahn, S. Huh, K. Kim, and S. Ahn, "A Coil Design and Control Method of Independent Active Shielding System for Leakage Magnetic Field Reduction of Wireless UAV Charger," *IEICE Trans. Commun.*, vol. E103.B, no. 9, pp. 889–898, Sep. 2020, doi: 10.1587/transcom.2019MCI0001.